Progress In Electromagnetics Research C, Vol. 116, 95–112, 2021

Design and Implementation of Long-Distance Dual PIFA Antenna Structure of Small Embedded Metal UHF RFID Tag

Zhidan Yan*, Shuchao Lu, Chao Zhang, and Zhenyu Yang

Abstract—As the advanced technology in the Internet of Things (IoT), ultra-high frequency radio frequency identification (UHF RFID) tag has broad application prospects and significant research value. However, the transmission performance of UHF RFID on the metal surface and embedded in metal is severely impaired, bringing new challenges to its application for long-distance reading and writing. On this basis, an embedded metal UHF RFID tag design method is proposed in this paper. A planar inverted F antenna (PIFA) structure is optimized to enhance the anti-metal performance of the tag. The embedded feed design is adopted to achieve preferable impedance matching between antenna and chip. Besides, a series of electromagnetic simulations were investigated to optimize the performance of the tag, which can ultimately achieve the maximum gain of $-9.7\,\mathrm{dB}$ in the metal groove, with the reduced volume of $19.8\,\mathrm{mm} \times 25.8\,\mathrm{mm} \times 2\,\mathrm{mm}$ by employing the meandering technology and the method of adding metal via holes. Finally, when the self-made tag is embedded in the metal groove, the experimental results demonstrate that the maximum reading distance can reach 1.26 m, indicating that the tag developed in this paper has significant practical value in the case of embedded metal.

1. INTRODUCTION

With the development of the Internet of Things (IoT), Radio Frequency Identification (RFID) technology is increasingly widely used in fields such as data exchange and object identification. UHF RFID technology has attracted much attention from researchers due to its fast recognition speed and long reading distance. However, the electric field around the UHF RFID tag will be significantly affected when the tag antenna works in the metal environment, decreasing the tag reading range [1].

To improve the performance of the tag antenna in the metal environment, many researchers have conducted a series of antenna structure optimization research and made much meaningful progress. Typically, Gao et al. used an Electromagnetic Band Gap (EBG) structure as a dielectric plate to improve the anti-metal performance of the tag antenna, revealing that the phase of the reflected wave from the metal surface would be deflected by the EBG structure, reducing the impact of metal on the antenna [2]. Hamzaoui et al. adopted an AMC structure for antenna design, verifying that its in-phase reflection characteristics can significantly improve antenna gain [3]. However, the application of the above two antennas is limited because of relatively complicated structures and high antenna manufacturing costs. Besides, Ukkonen et al. designed a microstrip patch antenna structure [4–6]. In [6], the impedance matching between the antenna and the tag chip can be achieved by adjusting the length of the feeder. The antenna performance can also be improved by adding a T-shaped matching structure [7] or an E-shaped groove [8] in the antenna. Agrawal et al. designed an asymmetric tri-band antenna, which can maintain good radiation performance on the car's surface, but its size is relatively large [9]. Additionally, the patch antenna design based on the electrical coupling between the radiating elements [10] can effectively weaken the influence of metal on the antenna. Furthermore, removing

Received 30 July 2021, Accepted 19 September 2021, Scheduled 10 October 2021
* Corresponding author: Zhidan Yan (zhidanyan@upc.edu.cn).
The authors are with the College of Control Science and Engineering, China University of Petroleum (East China), China.

short-circuit pins and ground layers [11] or adopting a planar structure [13] can reduce the cost of the tag. Making the radiating patch and feeding structure on the same plane [12] or using an open stub line feed planar antenna structure [13] can achieve an ideal impedance matching effect. Moh et al. adjusted the impedance of the antenna through the stub formed by folding two short induction tubes, and the designed antenna exhibited acceptable anti-metal performance on a metal surface [14]. Ng et al. proposed an E-shaped folded patch antenna structure that can quickly achieve tuning by adjusting 8 parameter values [15] while the antenna thickness is relatively large. Zhang and Long put forward two double-layer antenna structures [16, 17]. In [16], the antenna not only has a smaller size but also enhances the radiation of the antenna. In [17], the antenna has an extremely wide impedance bandwidth. However, the size is too large. Li et al. solved the problem of complex double-layer antenna structure and designed a single-layer tag antenna [18]; its structure is compact but not flexible enough. Goudos et al. used the improved bee colony algorithm to miniaturize the tag antenna and achieved good results [19]. Byondi et al. also presented a novel cavity tag antenna, demonstrating that the antenna can obtain longer reading distance than the existing passive tag antenna [20].

Considering that the RFID tags installed on the surface of products are exposed to the external environment, making the tags easy to be damaged intentionally or naturally, more and more product management put forward the application requirements of embedded metal RFID tags. Thus, it has become a new goal for researchers to design an RFID tag with a small size, long reading and writing distance, and being suitable for an embedded metal application environment. Kwon and Lee proposed a PIFA antenna structure, which easily matches most tag chips and has a long reading and writing distance [21]. Besides, Kim and Yeo presented a cavity-backed bow-tie antenna that can quickly achieve impedance matching using the coupling effect; the thickness of the dielectric substrate used was only 1.63 mm, and the antenna can be used in a metal groove [22]. Nevertheless, this antenna design was required to consider too many coupling problems between the antenna and the metal cavity, and the method was highly complicated. Additionally, Siden et al. provided an antenna with a smaller size [23], which was unsuitable for large-scale manufacturing due to its narrow bandwidth and high manufacturing tolerances.

Remarkably, the PIFA structure is evolved from a microstrip antenna, and its radiating patch and grounding plate are connected by short pieces. It not only has the typical characteristics of a microstrip antenna but also has the advantages of wide frequency band, compact structure, and low cost. In this paper, through detailed theoretical analysis and in-depth simulation research, an embedded anti-metal tag with a dual PIFA antenna structure and long-distance reading and writing ability is designed based on the improvement of the PIFA antenna. Regarding the antenna design, the feed patch adopts an embedded structure that adjusts the antenna input impedance by changing the embedded length and width; the antenna volume is reduced by introducing the meandering technology and substrate via hole method. Simulated and experimental results indicate that the designed RFID tag has a long reading and writing distance, meeting the needs of on-site industrial applications.

The rest of this paper is arranged as follows. The second section describes the relevant theories of tag antenna design and conducts the model selection analysis of the dielectric substrate. The third section details the basic structure of the antenna and the transmission line model. The fourth section provides the modeling and simulation results of the two distinctive situations (the metal groove is not embedded and is embedded) and analyzes the effect of each parameter on the antenna performance. The fifth section presents the actual test results of the antenna and performs the comparative analysis. Finally, a conclusion is drawn in the sixth section.

2. ANTENNA DESIGN BASIS

2.1. Tag Antenna Performance Parameters

The equivalent circuit when the tag antenna is working is illustrated in Fig. 1. V_a represents the equivalent source by the tag antenna receiving electromagnetic energy; $Z_a = R_a + jX_a$ denotes the complex impedance of the tag antenna; and $Z_c = R_c + jX_c$ indicates the complex impedance of the tag chip. The power transmission coefficient τ is usually used to characterize the degree of impedance

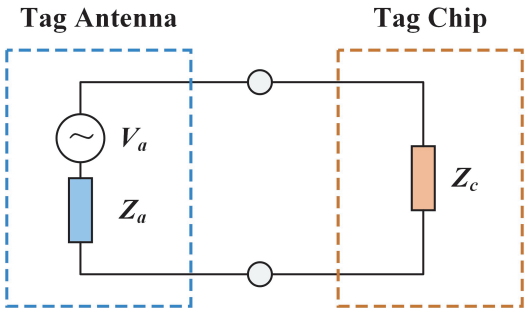

Figure 1. Tag antenna equivalent circuit.

matching:

$$\tau = \frac{P_c}{P_a} = \frac{4R_aR_c}{|Z_a + Z_c|^2}, \quad 0 \le \tau \le 1 \tag{1}$$

where P_c is the maximum power that the tag chip obtains from the tag antenna; P_a is the maximum power that the tag antenna obtains from the reader; R_a and Z_a represent the resistance and complex impedance of the tag antenna, respectively; R_c and Z_c denote the resistance and complex impedance of the tag chip, respectively. In Eq. (1), when the complex impedance of the tag antenna and the tag chip meet the conjugate matching condition, the power transmission coefficient is equal to 1, and there is the maximum transmission power between the antenna and the chip.

Therefore, the best matching condition for the equivalent circuit of the tag antenna is:

$$Z_a = Z_c^* \tag{2}$$

That is:

$$\begin{cases} R_a = R_c \\ X_a = -X_c \end{cases} \tag{3}$$

Particularly, the maximum reading distance R_{tag} of the tag antenna is a crucial parameter for evaluating the performance of the tag antenna. This parameter takes the smaller value between the maximum distance of tag activation and the maximum distance of the backscattered signal detected by the reader. Under normal circumstances, the sensitivity of the tag chip is much greater than that of the reader chip. Consequently, the tag activation distance is less than the maximum distance for the reader to detect the backscattered signal. Therefore, R_{tag} is determined by the tag activation distance derived from the Friis transmission equation:

$$R_{tag} = \frac{\lambda}{4\pi}\sqrt{\frac{P_tG_tG_rp}{P_r}} = \frac{\lambda}{4\pi}\sqrt{\frac{EIRP * G_r(1 - |S_{11}|^2)p}{P_{th}}} \tag{4}$$

where λ denotes the working wavelength; G_r indicates the gain of the tag antenna; S_{11} denotes the voltage reflection coefficient; P_{th}($P_{th} = P_r * \tau$, where P_r refers to the received power of the tag; τ is the power transmission coefficient) is the reading sensitivity of the tag chip; $EIRP$ ($EIRP = P_t * G_t$, where P_t is the transmit power of the reader; G_t represents the gain of the reader antenna) represents the equivalent isotropic radiation power. When $S_{11} = 0$, the impedances of the tag antenna and tag chip are completely matched, and the maximum value of R_{tag} is taken, suggesting that the polarizations of the tag antenna and the reader antenna are completely matched. In practical applications, the tag antenna and reader antenna generally do not meet the conditions of complete polarization matching. Thus, the polarization matching factor p is introduced to modify:

$$p = \frac{1 + \rho_1^2\rho_2^2 + 2\rho_1\rho_2\cos(\theta_1 - \theta_2)}{(1 + \rho_1^2)(1 + \rho_1^2)} \tag{5}$$

where ρ_1 and ρ_2 represent the axial ratios of the reader antenna and tag antenna, respectively; θ_1 and θ_2 denote the inclination angles of the polarization ellipse of the reader antenna and tag antenna, respectively.

It can be observed from Eq. (4) that keeping other parameters unchanged, the tag reading distance is positively correlated with antenna gain G_r and working wavelength λ and negatively correlated with S_{11}. In practical applications, the polarization form of most reader antennas is circular polarization, while the polarization form of tag antennas is often linear polarization. At this time, the polarization matching factor p between reader antenna and tag antenna can be taken as 0.5, and R_{tag} is reduced to $\sqrt{2}/2$ times the value under the perfect match condition.

In addition to impedance matching and the maximum reading distance, the antenna pattern and gain are also essential parameters affecting antenna performance. Generally, the dielectric material has a guiding effect on the antenna pattern, and the antenna pattern will tilt toward the direction of the dielectric material. However, the antenna pattern will tilt to the side away from the metal material because the metal material has a reflection effect on electromagnetic waves. For antenna gain, the larger the antenna size is, the greater the gain is. On the contrary, the smaller the thickness or the loss tangent of the tag dielectric substrate is, the greater the antenna gain is. Besides, the antenna gain would also be influenced by the surface area of the metal object, and the effect on the antenna gain can be ignored when the surface area of the metal object is large enough.

2.2. Dielectric Substrate Selection Analysis

It can be concluded from Section 2.1 that wavelength λ is a crucial parameter influencing the antenna reading distance. When the electromagnetic wave emitted by the antenna propagates in the medium, its wavelength λ is expressed as:

$$\lambda = \frac{\sqrt{2}}{f\sqrt{\mu\varepsilon}}\left[\sqrt{1+\left(\frac{\sigma}{\omega c}\right)^2}+1\right]^{-\frac{1}{2}} \tag{6}$$

where f is the frequency of electromagnetic waves; μ is the magnetic permeability of the antenna material; ε is the dielectric constant of the dielectric substrate; σ is the conductivity of the dielectric substrate; ω is the angular frequency; c is the speed of light (3×10^8 m/s). In Eq. (6), the working wavelength λ of the antenna is inversely proportional to $\sqrt{\varepsilon}$, and the size of the antenna is proportional to λ. Thus, a high-permittivity dielectric substrate is selected to reduce λ when a small antenna is designed, resulting in a decrease on the antenna size. Besides, if the conductivity σ is too large, the loss of electromagnetic waves during transmission in the dielectric substrate will increase, hindering long-distance information transmission. Therefore, it is reasonable to choose a dielectric substrate with low conductivity. After comprehensive consideration, TP-2 microwave composite dielectric material is adopted in this paper. It has a relative dielectric constant of 10.2 and a loss tangent of 0.003, which can meet the design requirements of miniaturization and remote reading and writing of RFID tags.

3. ANTENNA STRUCTURE AND TRANSMISSION LINE MODEL

3.1. Basic Structure of the Antenna

The tag antenna adopts a TP-2 dielectric substrate with a thickness of 2 mm. The antenna radiation surface is composed of two symmetrical PIFA patches on the dielectric substrate, and the back is a metal ground plane. Both are made of copper foil with a thickness of 0.035 mm. Simultaneously, metal via holes are provided in the dielectric substrate. Besides, the tag chip model is Alien Higgs 4; the equivalent input impedance of the chip is $Z_c = 18.4 - j181\,\Omega$ when the working frequency is $f = 915$ MHz; the chip is placed between the two patches to power the antenna. The specific structure is illustrated in Fig. 2, and the initial dimensions [24] of the tag antenna are provided in Table 1.

Particularly, the following optimizations were performed when the tag antenna is designed:

1) Multiple slots are made on the antenna patch according to the basic principle of meandering technology, making it effectively extend the current flow path to reduce the size of the antenna.

2) Adopt high dielectric constant dielectric substrate.

3) Metal via holes are opened on the dielectric substrate to realize the electrical connection between the antenna radiation patch and the metal ground plane; this can not only effectively avoid the weakening

Table 1. Structural parameters of the initial model of the tag antenna.

Design Variable	Parameter Meaning	Parameter Size (mm)
Patch_L	Patch length	20
Patch_W	Patch width	12
Gap_L	Gap Length	8
Gap_W	Gap Width	0.5
Inset_L	Insert Depth	2
Inset_W	Insert Width	1

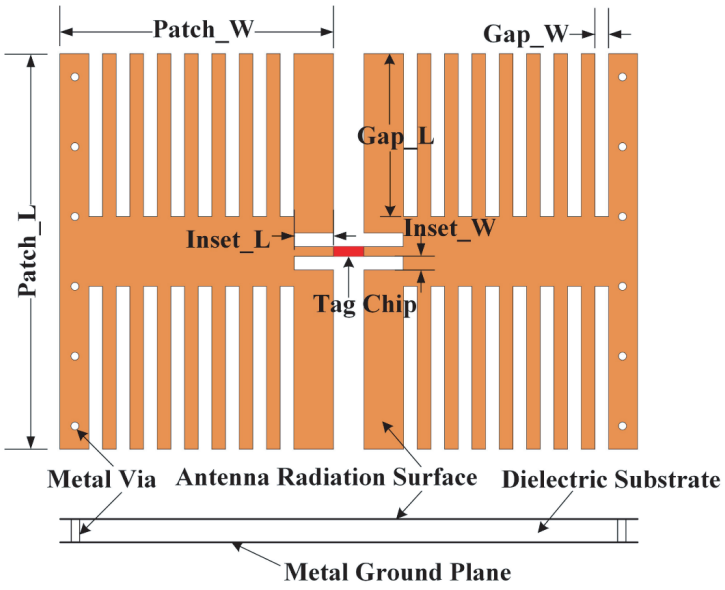

Figure 2. Tag antenna structure.

effect of the current intensity on the short-circuit patch by the sidewall of the metal groove but also form a standing wave from short to open, further reducing the antenna size.

3.2. Antenna Transmission Line Model

The equivalent transmission line model of the antenna is illustrated in Fig. 3. The radiating patches at both ends of the tag chip are regarded as a transmission line of length l. Then, the antenna input

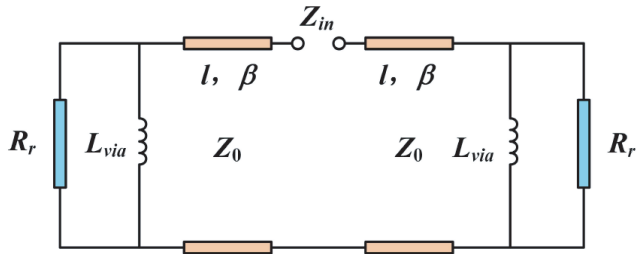

Figure 3. Tag antenna transmission line model.

impedance Z_{in} can be obtained as:

$$Z_{in} = 2Z_0 \frac{Z + jZ_0 \tan(\beta l)}{Z_0 + jZ \tan(\beta l)} \tag{7}$$

where Z_0 is the characteristic impedance of the radiation patch; $Z(Z_L//R_r)$ is the load impedance; $Z_L\,(j\omega L_{via})$ is the impedance of the metal via hole; R_r is the radiation resistance of the patch; β is the propagation constant.

According to Eq. (7), Z_{in} will be inevitably changed when the size of the antenna is changed. For the antenna design, Z_0 and R_r can be changed by reasonably adjusting the size of the embedded structure, causing the alteration in Z_{in} to achieve impedance matching between the tag antenna and tag chip.

4. MODELING AND SIMULATION

4.1. Finite Element Modeling

The tag antenna is modeled according to the dimensions provided in Table 1 by finite element method as illustrated in Fig. 4. Two copper sheets are added as the antenna radiation surface on a dielectric substrate with a size of 20 mm × 25.8 mm × 2 mm, and multiple gaps are added to the copper sheet depending on the meandering technique. The feeding part adopts an embedded structure, and the tag chip is placed in the middle of the embedded structure of the two antenna radiation patches for feeding. Simultaneously, a copper sheet is added at the bottom of the dielectric substrate as a metal ground plane to simulate the working condition of the antenna on the metal surface. Besides, the corresponding tag antenna's operating frequency is set to 915 MHz, and the input impedance is set to $Z_a = 18.4 - j181$.

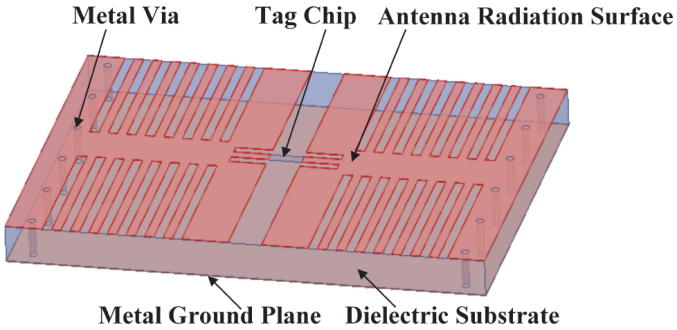

Figure 4. Modeling of the tag antenna.

4.2. Simulation Analysis of Tag Antenna When Not Embedded in the Metal Groove

First, the influence of the radiation patch size on the voltage reflection coefficient S_{11} is investigated when the tag is not embedded in the metal groove. The size of the S_{11} parameter can be used as a criterion for evaluating the transmitting efficiency of the antenna. Specifically, the higher the value of S_{11} is, the greater the energy reflected by the antenna itself is, the worse the impedance matching degree is, and the lower the transmission efficiency of the antenna is; otherwise, the higher the transmission efficiency of the antenna is. As presented in Fig. 5(a), with the increase of the patch length (Patch_L), the antenna resonance frequency increases, and the lowest point of S_{11} decreases, indicating that the increase of patch length can not only increase the equivalent wavelength of the antenna but also improve the impedance matching degree of the antenna. In Fig. 5(b), the antenna resonant frequency decreases as the patch width (Patch_W) increases; this is the opposite of patch length's effect on the resonant frequency.

The simulation results of the antenna S_{11} curve when the size of the radiation gap changes are illustrated in Fig. 6. It can be observed from Fig. 6(a) that the change of the radiation gap length

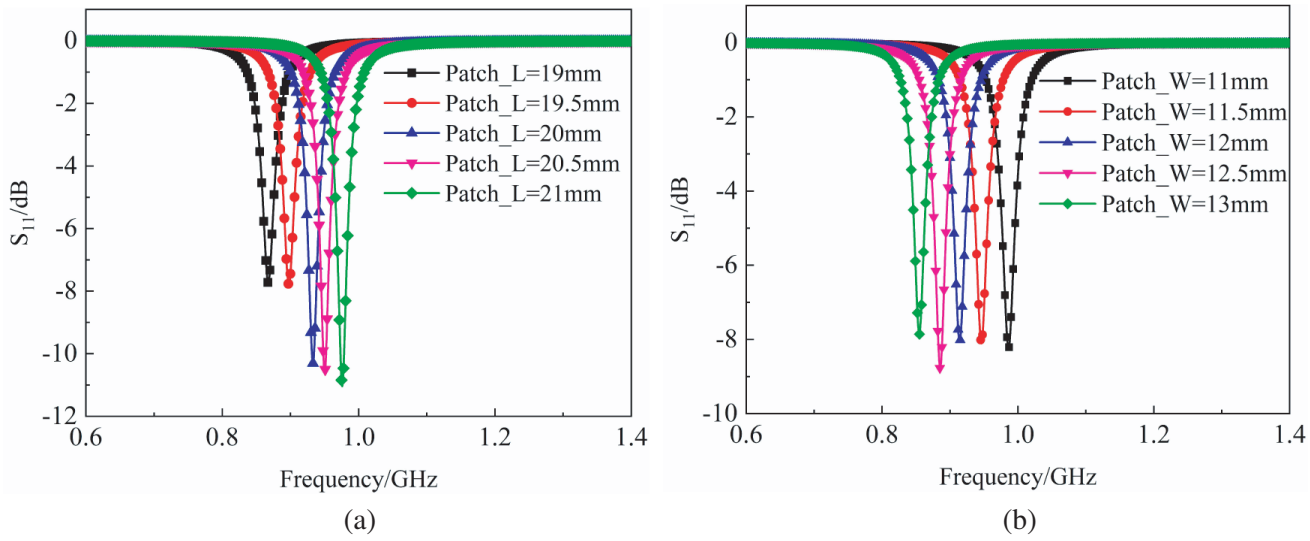

Figure 5. Effects of the patch size on the tag antenna S_{11}: (a) length and (b) width.

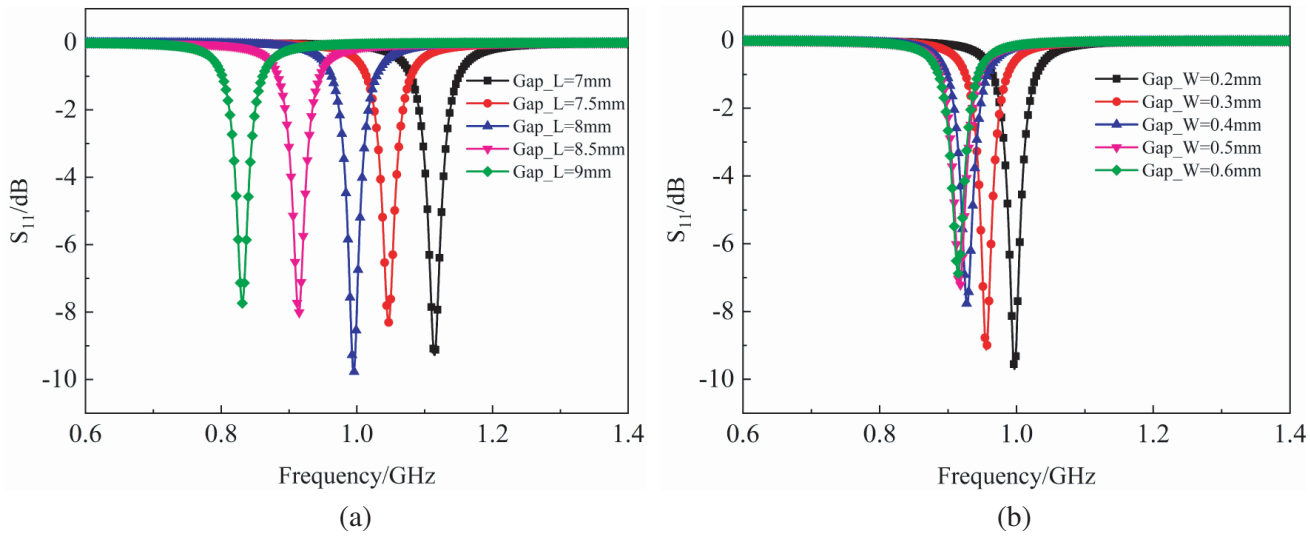

Figure 6. Effects of the radiation gap on the tag antenna S_{11}: (a) length and (b) width.

(Gap_L) causes the equivalent electrical length of the tag to change quickly due to a large number of radiation gaps; consequently, the resonance frequency has an extensive range of about 285 MHz. Besides, with the increase in Gap_L, the antenna resonance frequency decreases from 1115 MHz to 830 MHz, and the 3 dB bandwidth of the antenna drops from 34 MHz to 28 MHz. As exhibited in Fig. 6(b), with the increase in the radiation gap width (Gap_W), the resonant frequency moves to low frequency, and the resonant frequency changes in a smaller range of about 82 MHz. Meanwhile, the lowest point of S_{11} gradually rises, showing that the degree of antenna impedance matching becomes worse.

Besides, the designed antenna is fed with an embedded structure, and the change in the size of the structure would affect the performance of the antenna. Thus, it is necessary to investigate and analyze it. The result of antenna impedance varying with the length (Inset_L) of the embedded structure is exhibited in Fig. 7, in which the resistance ((a)) and reactance ((b)) of the antenna do not change significantly with the changes in Inset_L. Relatively, the embedded width (Inset_W) has a more significant impact on the impedance. As illustrated in Fig. 8, the resistance and reactance of the

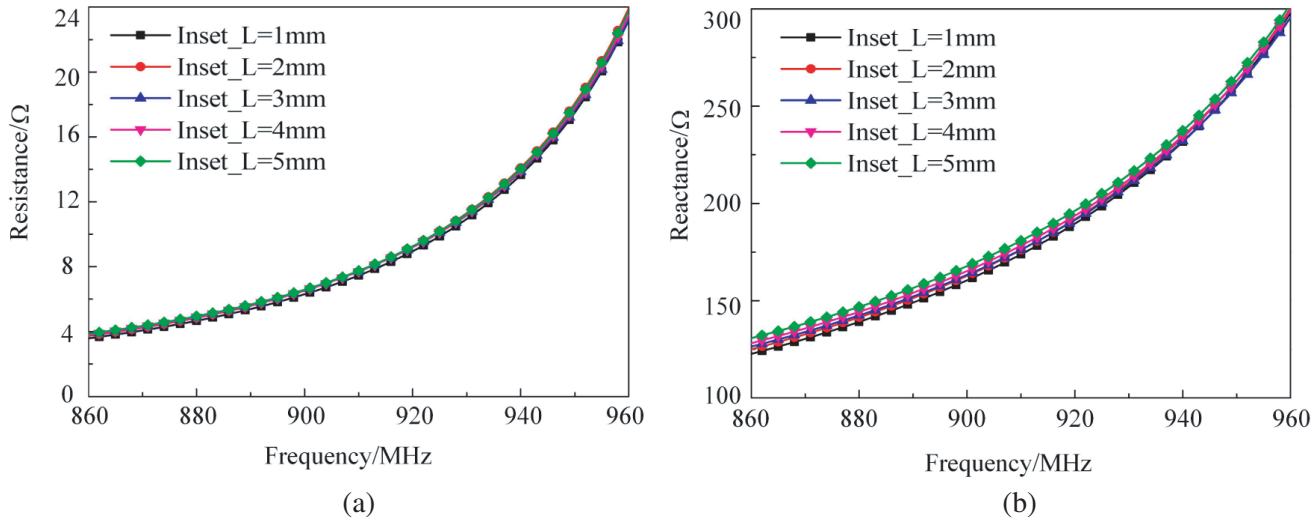

Figure 7. Effects of the embedded length on the tag antenna impedance: (a) resistance and (b) reactance.

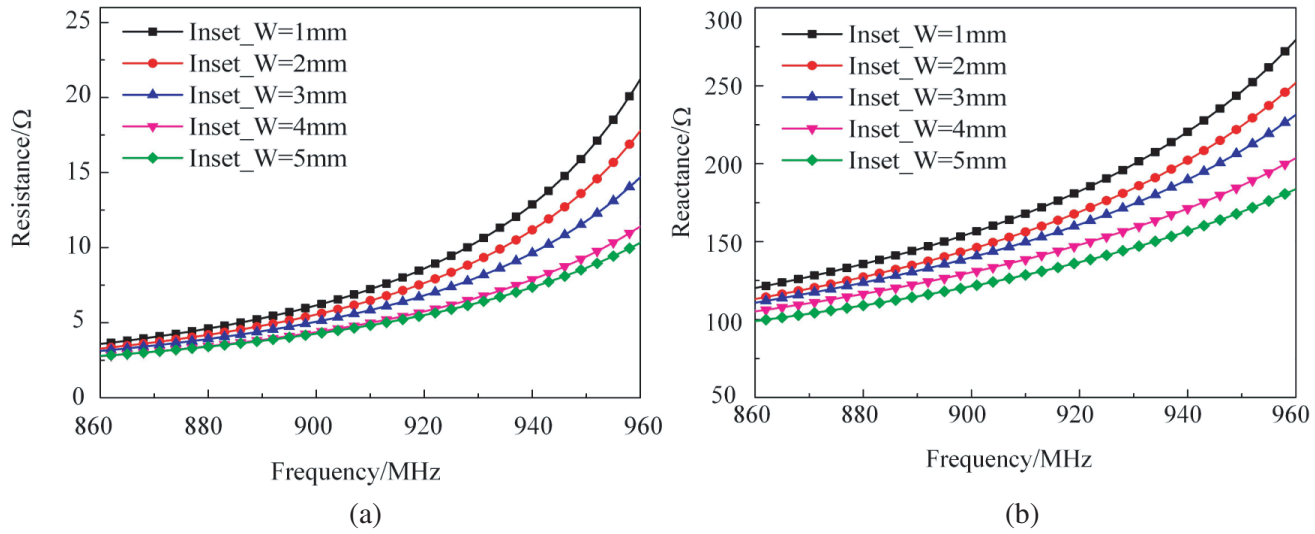

Figure 8. Effects of the embedded width on the tag antenna impedance: (a) resistance and (b) reactance.

antenna gradually decrease as Inset_W increases. At 915 MHz, the resistance of the antenna changes from 7 Ω to 5 Ω, and the reactance changes from 175 Ω to 133 Ω.

It can be observed from the above simulation analysis results that the resonant frequency of the antenna can be effectively adjusted by changing the size of the patch and the length of the radiation gap. On the contrary, the change of the radiation gap width has little effect on the antenna's resonant frequency, enabling it to fine-tune the resonant frequency of the antenna. Additionally, the input impedance of the antenna can be effectively adjusted by changing the width of the embedded structure, making the impedance matching between the tag antenna and the chip more flexible and improving the conjugated impedance matching degree of the tag antenna and the tag chip. Thus, reasonable adjustment of these parameters has excellent guiding significance for designing the ideal antenna.

4.3. Simulation Analysis of Tag Antenna When Embedded in the Metal Groove

Aiming at the situation where the tag antenna is embedded in the metal groove, the influence of three parameters (the depth of the metal groove, the lateral distance of the metal groove ⟨the distance between the tag and the sidewall of the metal groove⟩, and the thickness of the packaging material) on the antenna performance is investigated, respectively. The simulation model with the tag antenna embedded in the metal groove is illustrated in Fig. 9(a), and the relative size of the tag placed in the metal groove is presented in Fig. 9(b), where Cavity_H is the depth of the metal groove; Slot_L is the lateral distance of the metal groove; and Resin_H is the packaging material thickness of the tag. In the simulation, the relative dielectric constant of the packaging material is set to 4.8, and the loss tangent value is set to 0.015, consistent with the dielectric properties of epoxy resin.

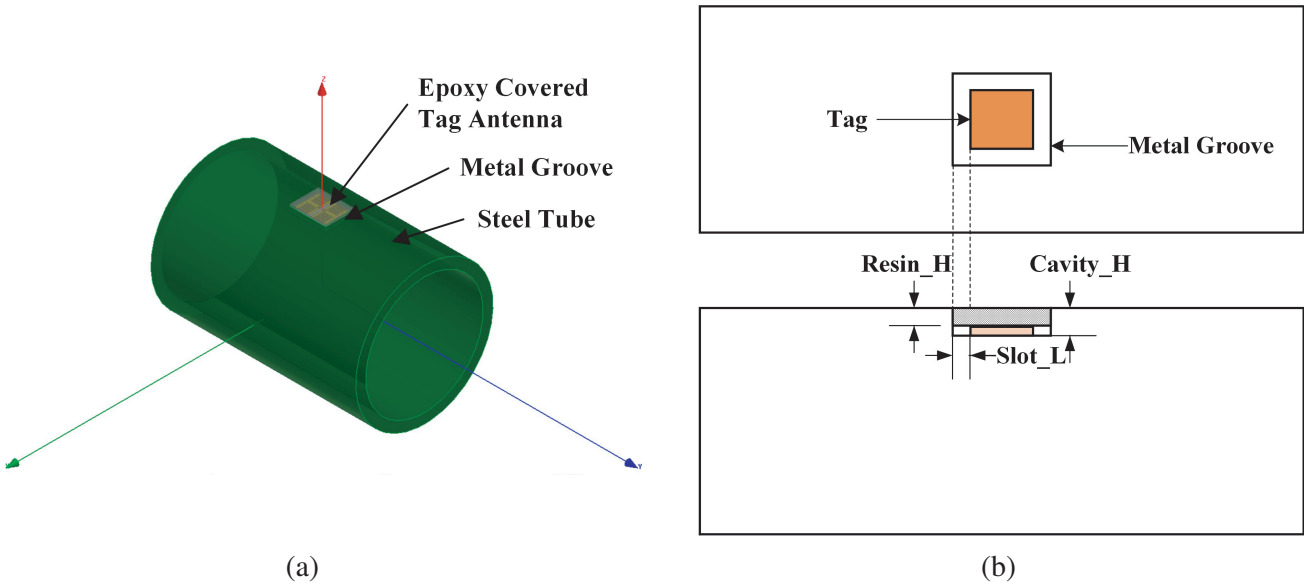

Figure 9. Simulation model and placement schematic diagram of the tag antenna in the metal groove: (a) simulation model and (b) placement schematic diagram.

The instantaneous amplitude distribution and vector diagram of the current density when the tag antenna works at 915 MHz are exhibited in Fig. 10. As observed in Fig. 10(a) and Fig. 10(b), the current is mainly concentrated in the middle of the radiation patch, tag chip, and metal ground plane. The high current density of the embedded structure indicates that the impedance of the antenna can be changed by adjusting the size of this structure. Fig. 10(c) illustrates that the current continuously flows in the opposite direction of the integration line, flows out from the metal via hole on the right, passes through the radiation patch and the tag chip to the metal via hole on the left, and finally flows back from the metal ground plane to the metal via hole on the right.

1) The influence of the depth of the metal groove

The influence of the depth of the metal groove on S_{11} and antenna gain is presented in Fig. 11. It can be observed from Fig. 11(a) that the lowest point of S_{11} decreases as Cavity_H increases, indicating that the antenna's impedance matching degree improves. However, the antenna resonance frequency also decreases from 983 MHz to 908 MHz, but this is not what is expected. Besides, the negative effect of the increase in the depth of the metal groove on the resonant frequency can be offset by reducing the antenna size because this way can effectively shorten the current flow path on the antenna and increase the resonant frequency of the antenna. As demonstrated in Fig. 11(b), the antenna gain decreases with the increase in Cavity_H; this is completely predictable. Additionally, the antenna gain decreases by about 1 dB for every 1 mm increase in the depth of the metal groove. Particularly, when Cavity_H is 4 mm, the antenna resonance frequency is exactly 915 MHz, then its maximum gain can reach −9.8 dB approximately.

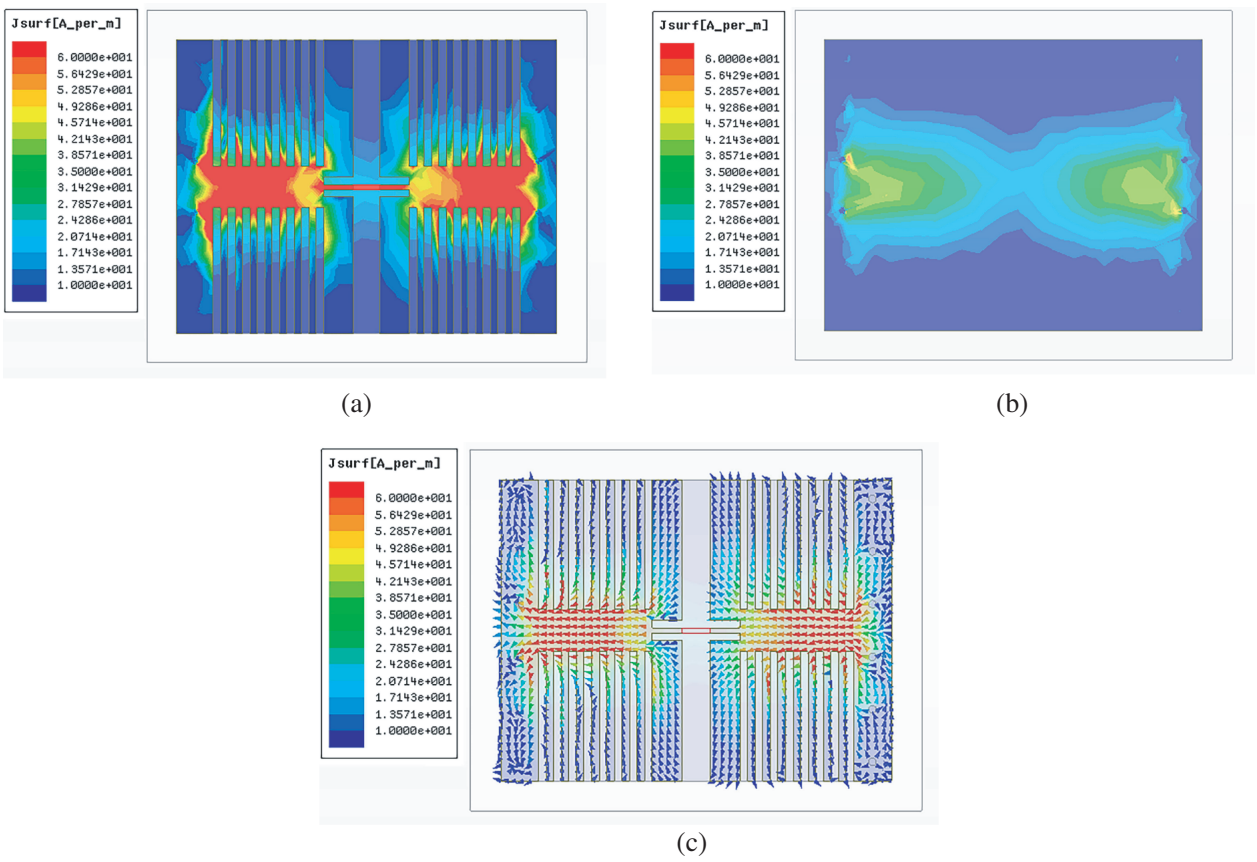

Figure 10. Instantaneous current density amplitude of the front and back of the tag antenna and vector diagram of current density: (a) the front side, (b) the back side, and (c) vector diagram.

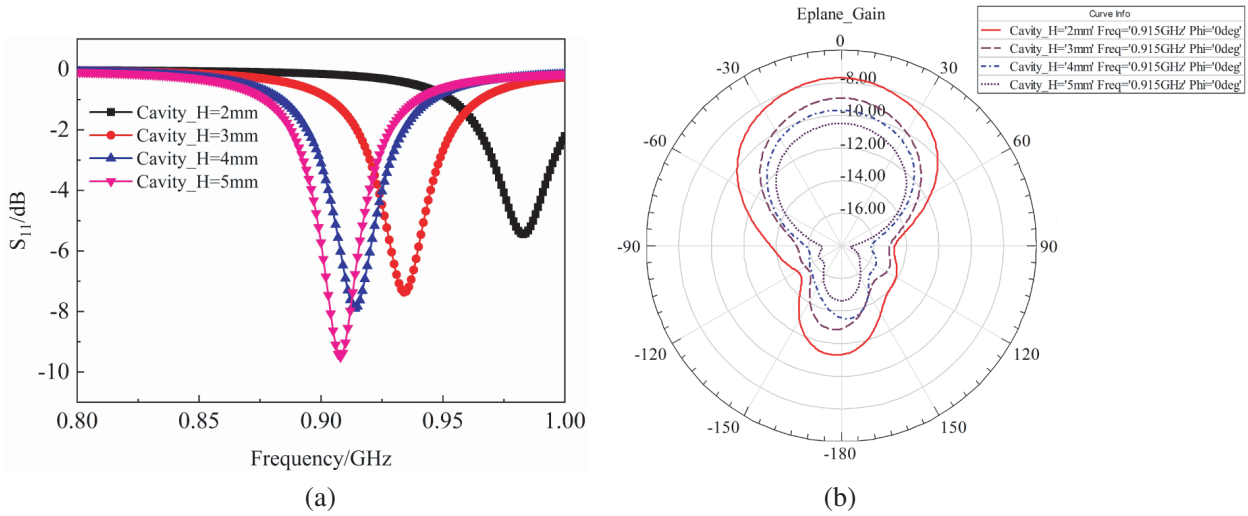

Figure 11. Effects of the depth of metal groove on the tag antenna S_{11} and gain: (a) S_{11} and (b) gain.

2) The influence of the lateral distance of the metal groove

The simulation results of the S_{11} parameters and antenna gain varying with the lateral distance of the metal groove (Slot_L) are provided in Fig. 12. When Slot_L changes from 1 mm to 2 mm, the resonant frequency of the antenna moves to high frequency; the lowest point of S_{11} rises (Fig. 12(a));

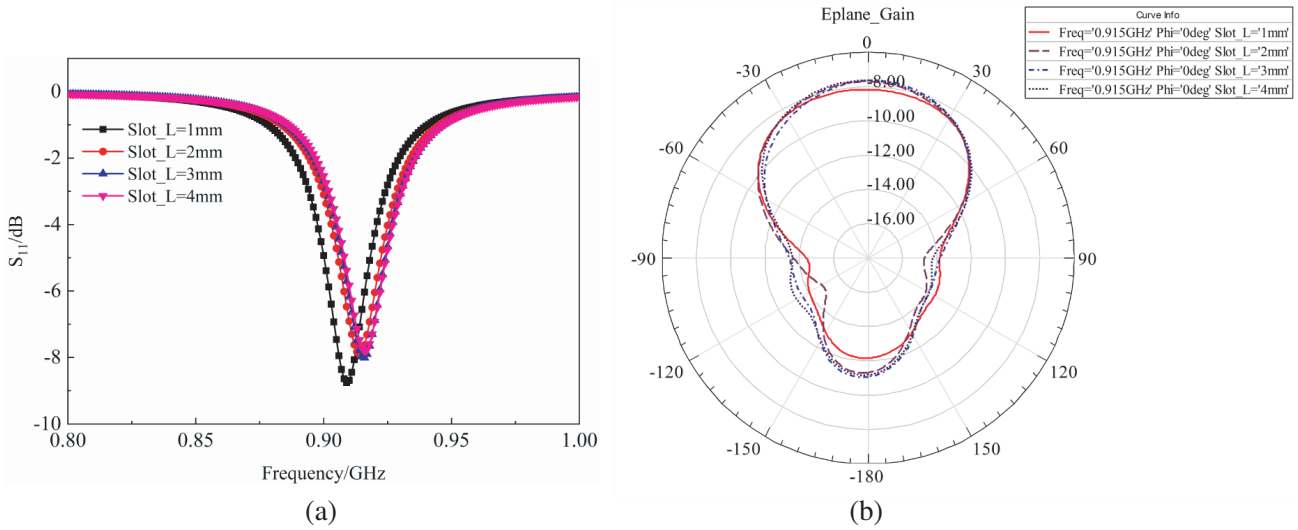

Figure 12. Effects of the lateral distance of metal groove on the tag antenna S_{11} and gain: (a) S_{11} and (b) gain.

and the vertical gain of the tag antenna increases (Fig. 12(b)). When Slot_L is changed from 2 mm to 4 mm, there is no significant change in the resonant frequency of the antenna, and the antenna gain has a similar trend. Simultaneously, the influence of Slot_L on the antenna is dramatically reduced.

3) The influence of packaging material and its thickness

The packaging material has a specific dielectric constant and loss tangent, which would affect the radiation performance of the tag antenna. According to related literature [25], epoxy resin has characteristics of low cost and high availability, and using it as an antenna encapsulation material can not only protect the antenna from the surrounding environment but also slightly improve the antenna performance. Besides, the epoxy resin also has satisfactory dielectric properties. Thus, the material consistent with the dielectric parameters of epoxy resin is selected in this paper for simulation analysis.

The results of the tag antenna S_{11} and antenna gain varying with the changes in packaging material thickness (Resin_H) are illustrated in Fig. 13. In Fig. 13(a), as Resin_H increases, the resonant frequency

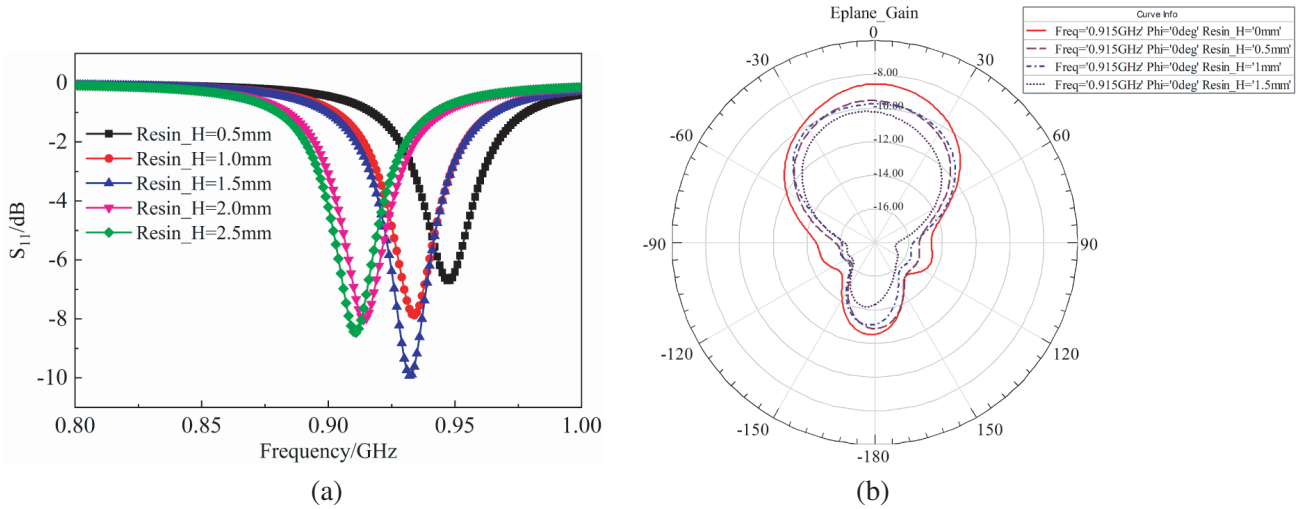

Figure 13. Effects of the packaging material thickness on the tag antenna S_{11} and gain: (a) S_{11} and (b) gain.

of the tag antenna significantly decreases, and the lowest point of S_{11} gradually decreases, indicating that the antenna's conjugate impedance matching degree improves. It is easy to predict that the thicker the packaging material is, the smaller the antenna gain is; the prediction result is provided in Fig. 13(b).

4.4. Anti-Metal Antenna Design Results

The final size of the tag antenna obtained using the simulation data is listed in Table 2. The size of the antenna is 19.8 mm × 25.8 mm × 2 mm. The actual physical tag antenna is displayed in Fig. 14. As the simulative studies recommended, the depth of the metal groove on the tubing is set to 4 mm, the lateral distance of the metal groove set to 2 mm, and the thickness of the packaging material set to 2 mm, respectively.

Table 2. Structural parameters of final model of the tag antenna.

Design Variable	Parameter Meaning	Parameter Size (mm)
Patch_L	Patch length	19.8
Patch_W	Patch width	12
Gap_L	Gap Length	8.5
Gap_W	Gap Width	0.5
Inset_L	Insert Depth	2
Inset_W	Insert Width	0.5

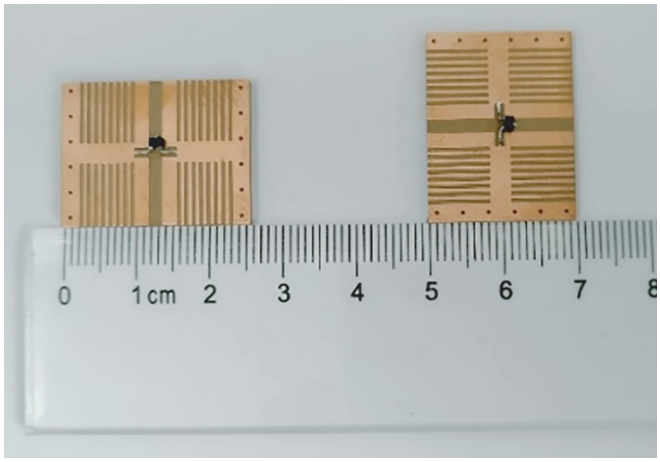

Figure 14. Physical tag antenna.

The simulation results of S_{11} curve and three-dimensional gain pattern of the tag antenna are illustrated in Fig. 15. It can be observed from Fig. 15(a) that in the operating frequency range of 902 ∼ 928 MHz, the tag antenna can cover both North America (902 ∼ 928 MHz) and China (920 ∼ 925 MHz) UHF RFID frequency band simultaneously. The impedance matching degree of the antenna is acceptable. Meanwhile, the 3 dB bandwidth, which is an important criterion for antenna performance evaluation [4, 12, 13, 16–18], reaches 30 MHz. As presented in Fig. 15(b), the maximum gain of the antenna reaches −9.7 dB. At the same time, the radiation efficiency of the antenna is about 0.054. More importantly, the tag antenna has preferable omnidirectionality above the metal groove, and the half-power beamwidth is about 100°, allowing it to achieve the reading and writing stability of the tag in a larger range. According to the calculation of the tag maximum reading distance by Eq. (4), the theoretical maximum reading distance of the tag is obtained to be about 2.1 meters.

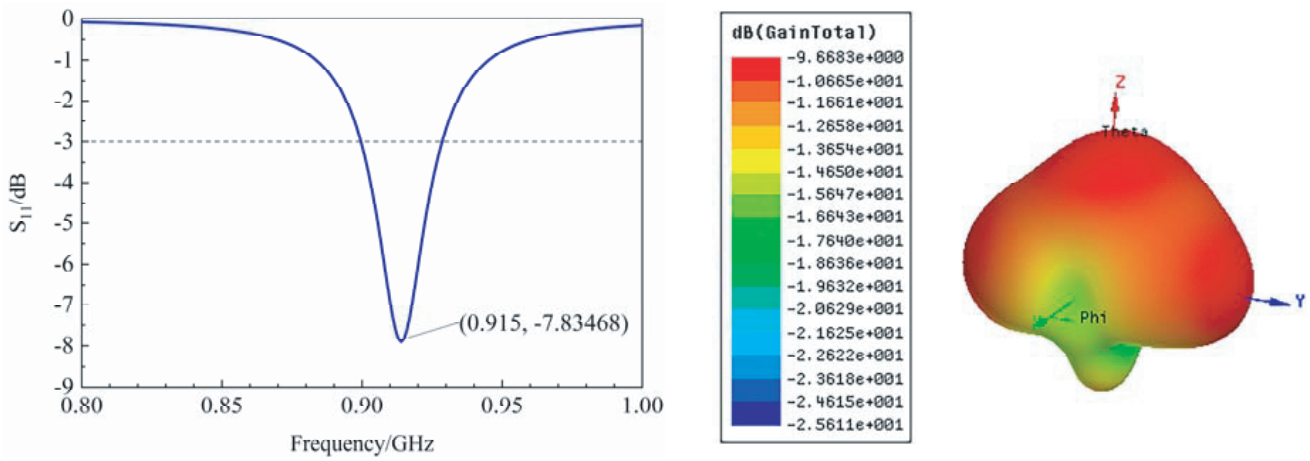

(a) (b)

Figure 15. S_{11} curve and three-dimensional gain pattern of the tag antenna: (a) S_{11} curve and (b) three-dimensional gain pattern.

5. RESULTS AND DISCUSSION

5.1. Tag Impedance Test

The data of S parameter are derived from a vector network analyzer using dual-port test method, drawn in Fig. 16. Because of the mismachining tolerance between the measured antenna and simulated antenna, and the error generated in the test process which introduces equivalent resistance and inductance into the antenna, the test value is a little larger than the simulation value. However, as illustrated in Fig. 16, with the increase of the sweep frequency from 860 MHz to 960 MHz, the input-resistance and input-reactance of the antenna rise monotonically from 12.6 Ω to 31.4 Ω, and from 143.6 Ω to 310.4 Ω, respectively, indicating the consistent trend compared with the simulation values.

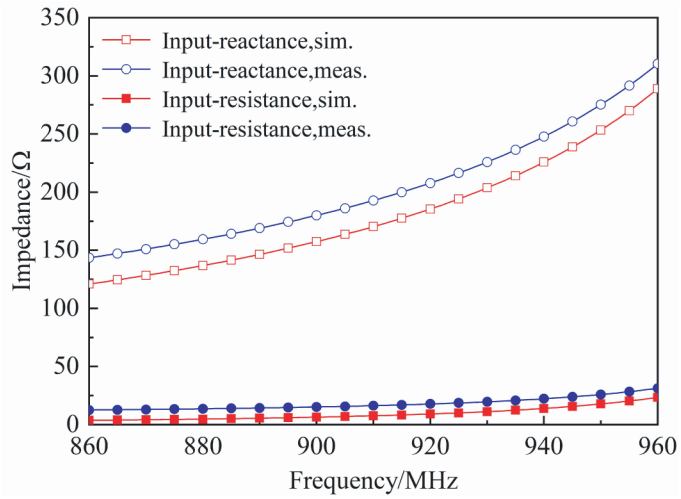

Figure 16. Input impedance versus frequency of the tag antenna.

5.2. Maximum Tag Reading Distance Test

Figure 17 illustrates the maximum reading distance test platform. Ljyzn-101 UHF fixed reader is used in the test, which has an antenna polarization mode of circular polarization and the maximum gain

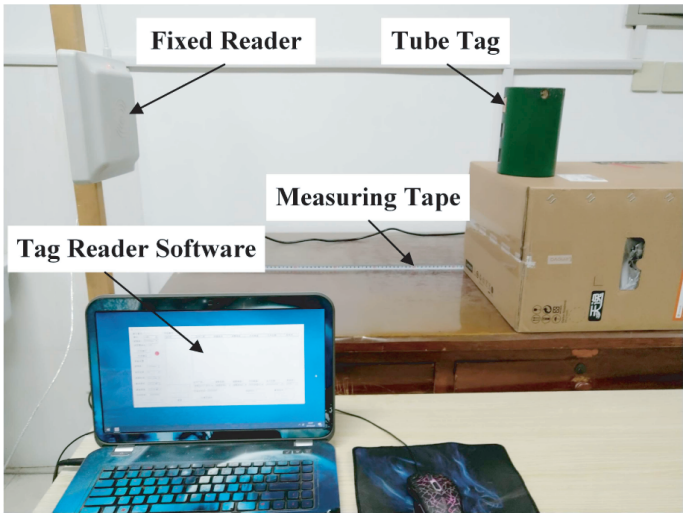

Figure 17. Field test platform.

of 8 dBi. Meanwhile, the tag and reader are at a certain height from the ground and on the same horizontal line to reduce the impact of the surrounding objects on the tag antenna and reader antenna. The tag antenna is embedded in the metal groove of the oil pipe. Additionally, the support part of the reader-writer and oil pipe in the test is composed of a wooden bracket and carton, and the packaging material of the tag in the metal groove adopts high-strength epoxy resin.

The test results of the maximum reading distance of the tag, when the metal groove has different depths and lateral distances, are illustrated in Fig. 18, respectively. The lateral distance of the metal groove is fixed to 2 mm. In Fig. 18(a), with packaging material, the maximum reading distance of the tag significantly changes when the depth of the metal groove changes from 3 mm to 5 mm, and the maximum reading distance of the tag reaches 126 cm when the depth of the metal groove is 4 mm. In the absence of packaging materials, the antenna resonance frequency and impedance change, resulting in a decrease in impedance matching between the tag antenna and the tag chip; consequently, the maximum reading distance of the tag does not change significantly and even decreases. Next, when the depth of the metal groove is fixed to 4 mm, it can be observed from Fig. 18(b) that whether there are packaging

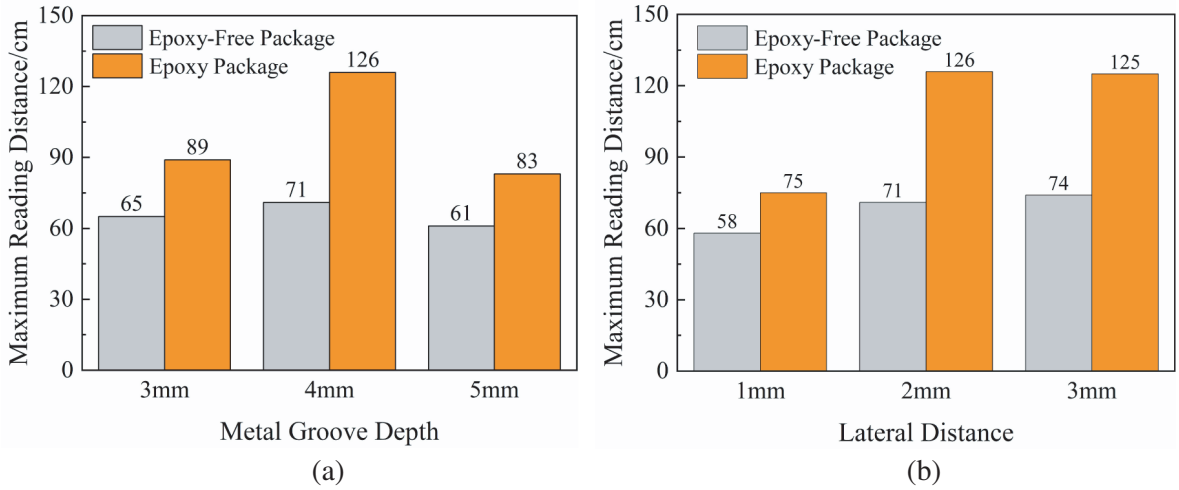

Figure 18. Maximum reading distances of the tag antenna in the metal groove with different depths and lateral distances: (a) depth and (b) lateral distance.

materials or not, the maximum reading distance of the tag increases when the lateral distance of the metal groove changes from 1 mm to 2 mm, and the maximum reading distance of the tag is almost unchanged when the lateral distance is greater than 2 mm, then it is found that the maximum reading distance of the tag is only 74 cm, which is much less than that with packaging material.

Finally, the depth of the metal groove is selected as 4 mm, and the lateral distance of the metal groove is selected as 2 mm. In the cases without packaging materials and with packaging materials, the maximum reading distance corresponding to each frequency point is tested when the tag changes from 902 MHz to 928 MHz. The test results are exhibited in Fig. 19. It can be discovered that the maximum reading distance of a tag without packaging materials is 80 cm at 930 MHz. After adding packaging materials, the maximum reading distance is 126 cm at 914 MHz, which is more than 50% higher than that without packaging materials.

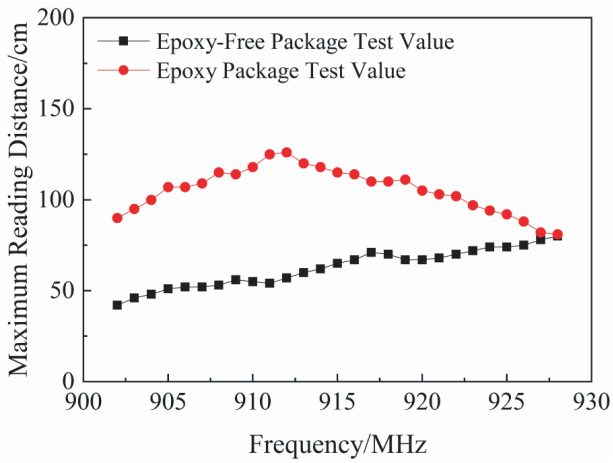

Figure 19. Maximum reading distance of tag antenna at different frequencies.

Particularly, the proposed antenna was also compared with other referenced anti-metal RFID tag antennas in Table 3 in terms of size, simulation reading distance, and bandwidth. In order to facilitate the comparison of the parameters between different antennas, EIRP is unified to a typical value of 2 W. From Table 3, the tag in [7] has poor performance in all aspects. The bandwidth of the tag in [16] is only 8 M, even if it has a similar size and a longer reading distance. The tags in [5, 17, 20] have longer reading distances and broader bandwidths than the proposed one, and the larger sizes limit their applications. Therefore, it is clear that the proposed antenna has its excellent comprehensive performance of a smaller size, an adequate bandwidth, and a workable long reading distance.

Furthermore, the maximum reading distance of the tag was tested on the surface of the carton and oil pipe, respectively, to simulate the working environment of the tag in free space and metal surfaces. The test results were 46 cm and 58 cm, respectively, which were less than the maximum reading distance

Table 3. Comparison of the proposed tag antenna with other anti-metal tags in references.

Item	Frequency (GHz)	Size (mm^3)	Simulation Reading Distance (m)	Bandwidth (MHz)
Proposed	0.915	$19.8 \times 25.8 \times 2$	2.1 (1.26 m Measured)	30
Ref. [5]	0.915	$100 \times 35 \times 3$	7.5	~ 50
Ref. [7]	0.921	$58 \times 34 \times 0.85$	1.7	~ 20
Ref. [16]	0.923	$26 \times 14 \times 2.4$	4.5	8
Ref. [17]	0.890	$56 \times 26 \times 3.2$	2.2	100
Ref. [20]	0.970	$140 \times 60 \times 10$	25.7	~ 50

of the tag in the metal groove. This is because the resonance frequency shifts will lead to poor impedance characteristics when the tag works in the free space or metal surface, making the maximum reading distance of the antenna drop. Concurrently, it is also discovered that the measured maximum reading distance has a certain deviation from the theoretical value when there is an epoxy resin package. The reasons are concluded as follows:

1) There are some errors in the actual manufacture of the tag antenna, the welding of the tag chip, and the test of reading distance;

2) There is a deviation between the actual value and simulation value of the dielectric constant of the antenna substrate and epoxy resin;

3) The laboratory test environment has more electromagnetic interference than the microwave anechoic chamber test environment;

4) During the test, there is an inevitable slight alignment deviation between the tag antenna's normal direction and the radiation direction of the maximum gain of the reader antenna.

6. CONCLUSION

This paper has presented a design method of embedded metal UHF RFID tags based on dual PIFA structure. Taking "theory-simulation-design-experiment" as the research idea and depending on the theoretical foundation of antenna design, the effects of the tag structural parameters and the key dimensions and packaging material of the metal groove with the embedded tag on the antenna performance have been emphatically investigated. On this basis, a small-size tag that can be embedded into metal has been designed and tested for its impedance and maximum reading distance. Finally, some meaningful conclusions have been acquired:

1) Theoretical analysis has revealed that the maximum transmission power between the antenna and the chip exists when conjugate matching is achieved; the tag reading distance is positively correlated with the antenna gain and working wavelength and negatively correlated with S_{11}; the introduction of polarization matching factor can more accurately correct the tag reading distance; TP-2 is selected as the tag dielectric substrate material after investigating the influence of the dielectric substrate characteristics on the working wavelength.

2) When the tag is not embedded in the metal groove, the antenna size significantly impacts the antenna performance parameters such as the length and width of the radiation patch, the length of the radiation gap, and the width of the embedded structure. For example, when the radiation gap length (Gap_L) increases from 7 mm to 9 mm, the resonant frequency of the antenna drops from 1115 MHz to 830 MHz, and the 3 dB bandwidth of the antenna decreases from 34 MHz to 28 MHz. When the width of the embedded structure (Inset_W) rises from 1 mm to 5 mm, at the frequency of 915 MHz; the resistance of the antenna drops from 7 Ω to 5 Ω; and the reactance decreases from 175 Ω to 133 Ω.

3) When the tag is embedded in the metal groove, the depth of the metal groove and the thickness of the packaging material have a more significant effect on the antenna performance than the lateral distance of the metal groove. For example, when the depth of the metal groove (Cavity_H) increases from 2 mm to 5 mm, the antenna resonance frequency decreases from 983 MHz to 908 MHz, and the antenna gain is reduced by about 3 dB. Particularly, when Cavity_H is 4 mm, the antenna resonance frequency is 915 MHz, and the maximum gain is approximately −9.8 dB.

4) In the antenna design, the feed patch adopts an embedded structure, and the input impedance of the antenna can be adjusted by changing the embedded structure length and width. Simultaneously, the antenna volume is effectively reduced by introducing meandering technology and the substrate via hole method, and the final size of the self-made tag is 19.8 mm × 25.8 mm × 2 mm.

5) Experimental tests have demonstrated that the self-made tag antenna has a preferable impedance matching with the tag chip, and the packaging material can effectively increase the reading distance of the self-made tag. When the lateral distance of the metal groove is 2 mm, the maximum reading distances of the tag without packaging materials and with packaging materials can reach 71 cm and 126 cm, respectively. Besides, the maximum reading distance of the tag becomes stable when the lateral distance of the metal groove exceeds 2 mm. Therefore, it can be considered that 2 mm is a suitable choice for the lateral distance of the metal groove, and the self-made tag can be applied to most embedded metal applications due to its large acceptable reading distance.

ACKNOWLEDGMENT

We would like to acknowledge the anonymous reviewers for their valuable suggestions and corrections and thank the financial support of the National Natural Science Foundation of China (Grant No. 52075546), Natural Science Foundation of Shandong Province (Grant No. ZR2020MA056), and Shandong Key R&D Program (Grant No. ZR2020MA056).

REFERENCES

1. Dobkin, D. M. and S. M. Weigand, "Environmental effects on RFID tag antennas," *IEEE MTT-S Int. Microw. Symp. Dig.*, 135–138, 2005.
2. Gao, B., C. H. Cheng, M. M. F. Yuen, and R. D. Murch, "Low cost passive UHF RFID packaging with Electromagnetic Band Gap (EBG) substrate for metal objects," *2007 Proceedings 57th Electronic Components and Technology Conference*, 974–978, 2007.
3. Hamzaoui, D., F. Djahli, T. P. Vuong, Q. V. H. Thi, and G. Kiani, "High gain long-read range AMC-backed tag antenna for european UHF RFID applications," *Microwave and Optical Technology Letters*, Vol. 58, No. 12, 2944–2948, 2016.
4. Ukkonen, L., M. Schaffrath, D. W. Engels, L. Sydanheimo, and M. Kivikoski, "Operability of folded microstrip patch-type tag antenna in the UHF RFID bands within 865–928 MHz," *IEEE Antennas and Wireless Propagation Letters*, Vol. 5, 414–417, 2006.
5. Tao, B., H. Sun, and O. M. Ramahi, "RFID tag antenna for metallic or non-metallic surfaces," *Progress In Electromagnetics Research C*, Vol. 59, 51–57, 2015.
6. Lee, B. and B. Yu, "Compact structure of UHF band RFID tag antenna mountable on metallic objects," *Microwave and Optical Technology Letters*, Vol. 50, 232–234, 2008.
7. Faudzi, N. M., M. T. Ali, I. Ismail, H. Jumaat, and N. H. M. Sukaimi, "Compact microstrip patch UHF-RFID tag antenna for metal object," *2014 IEEE Symposium on Wireless Technology and Applications (ISWTA)*, 2014.
8. He, Y. and Z. Pan, "Design of UHF RFID broadband anti-metal tag antenna applied on surface of metallic objects," *2013 IEEE Wireless Communications and Networking Conference (WCNC)*, 4352–4357, 2013.
9. Agrawal, N., A. K. Gautam, and K. Rambabu, "Design and packaging of multi-polarized triple-band antenna for automotive applications," *AEU — International Journal of Electronics and Communications*, Vol. 113, 1434–8411, 2020.
10. Yu, B., S. J. Kim, B. Jung, F. J. Harackiewicz, and B. Lee, "RFID TAG antenna using two-shorted microstrip patches mountable on metallic objects," *Microwave and Optical Technology Letters*, Vol. 49, 414–416, 2010.
11. Cho, C., H. Choo, and I. Park, "Design of planar RFID tag antenna for metallic objects," *Electronics Letters*, Vol. 44, 175–177, 2008.
12. Kim, J. S., W. K. Choi, and G. Y. Choi, "Small proximity coupled ceramic patch antenna for UHF RFID tag mountable on metallic objects," *Progress In Electromagnetics Research C*, Vol. 4, 129–138, 2008.
13. Mo, L. and C. Qin, "Planar UHF RFID tag antenna with open stub feed for metallic objects," *IEEE Transactions on Antennas and Propagation*, Vol. 58, 3037–3043, 2010.
14. Moh, C., E. Lim, F. Bong, and B. Chung, "Miniature coplanar-fed folded patch for metal mountable UHF RFID tag," *IEEE Transactions on Antennas and Propagation*, Vol. 66, 2245–2253, 2018.
15. Ng, W., E. Lim, F. Bong, and B. Chung, "E-shaped folded-patch antenna with multiple tuning parameters for on-metal UHF RFID tag," *IEEE Transactions on Antennas and Propagation*, Vol. 67, 56–64, 2019.
16. Zhang, J. and Y. Long, "A novel metal-mountable electrically small antenna for RFID tag applications with practical guidelines for the antenna design," *IEEE Transactions on Antennas and Propagation*, Vol. 62, 5820–5829, 2014.

17. Zhang, J. and Y. Long, "A dual-layer broadband compact UHF RFID tag antenna for platform tolerant application," *IEEE Transactions on Antennas and Propagation*, Vol. 61, 4447–4455, 2013.
18. Li, H., J. Zhu, and Y. Yu, "Compact single-layer RFID tag antenna tolerant to background materials," *IEEE Access*, Vol. 5, 21070–21079, 2017.
19. Goudos, S. K., K. Siakavara, and J. N. Sahalos, "Design of load-ended spiral antennas for RFID UHF passive tags using improved artificial bee colony algorithm," *AEU — International Journal of Electronics and Communications*, Vol. 69, 206–214, 2015.
20. Byondi, F. K. and Y. Chung, "Longest-range UHF RFID sensor tag antenna for IoT APPLIED FOR METAL AND NON-METAL OBJects," *Sensors*, Vol. 19, 2019.
21. Kwon, H. and B. Lee, "Compact slotted planar inverted-F RFID tag mountable on metallic objects," *Electronics Letters*, Vol. 41, 1308–1310, 2005.
22. Kim, D. and J. Yeo, "A passive RFID tag antenna installed in a recessed cavity in a metallic platform," *IEEE Transactions on Antennas and Propagation*, Vol. 58, 3814–3820, 2010.
23. Siden, J. and H. E. Nilsson, "An electrically small elliptic PIFA for RFID in harsh metallic environments," *IEEE International Conference on Microwaves*, 2013.
24. Kim, J. S., W. Choi, and G. Y. Choi, "UHF RFID tag antenna using two PIFAs embedded in metallic objects," *Electronics Letters*, Vol. 44, 1181–1182, 2008.
25. Vera-Dimas, J. G., M. Tecpoyotl-Torres, V. Grimalsky, S. V. Koshevaya, and J. A. García-Limón, "Experimental analysis of epoxy resin as antenna radome," *2012 19th International Conference on Microwaves, Radar & Wireless Communications*, 176–179, 2012.